Superposition of noncoaxial vortices in parametric wave mixing

Anatoly P. Sukhorukov* and Alexey A. Kalinovich
Laboratory of Nonlinear Waves, Radiophysics Department, Physics Faculty, Moscow State University, Moscow 119899, Russia

Gabriel Molina-Terriza† and Lluis Torner
Department of Signal Theory and Communications, Universitat Politecnica da Catalunya, Gran Capitan UPC-D3 Barcelona ES 08034, Spain
(Received 27 June 2002; published 19 September 2002)

In this paper we present a comprehensive study of the dynamics of screw phase dislocations under conditions of noncoaxial parametric three-wave mixing in the pump low-depletion regime. Under such conditions the signal and idler fields couple and so, the fields' properties change through propagation in the nonlinear crystal. We present an analytical model and a comprehensive study of the vortical features of the resulting field. The model is compared with the numerical solutions of the full equations. It is shown that by changing the relative amplitude and phase of the initial fields, one can control the domains where creation and annihilation of vortex-antivortex twins lead to different vortex content. We show that the effects studied here are relevant to a variety of physical systems. In particular, we show that the same phenomena are expected to occur in gyrotropic media and photonic crystals.

DOI: 10.1103/PhysRevE.66.036608 PACS number(s): 42.65.Tg, 42.65.Ky

I. INTRODUCTION

Since screw dislocations were first discussed in general wave fronts [1], the study of these structures has grown to become a field of its own: singular optics [2–6]. Optical screw dislocations, also called optical vortices, are singularities in the wave front of an optical field, where the amplitude vanishes and the phase twists around the singularity taking all possible values. The number of twists of the phase, modulo 2π is called the topological charge of the vortex, which can be either positive or negative depending on the direction of the twist. Vortices appear spontaneously in several settings, and otherwise they can be generated with phase masks [7,8], or with astigmatic optical components [9].

In this context, parametric mixing of multiple waves containing wave front dislocations in quadratic nonlinear media constitutes a fascinating scenario. Because of the parametric interaction, the waves exchange not only energy with each other but also nonlinear phase shifts, hence wave fronts. The dislocations can be transformed from one frequency to another. In particular, they can be converted to the second harmonic [10–14] and to the sum frequency wave [15]. In all cases studied to date, the pump beams contained coaxial vortices. Thus, the investigation of the superposition of noncoaxial vortices in parametrically coupled waves remains open.

Actually, even the linear superposition of coaxial [16] and noncoaxial [17] vortical fields exhibits much richer properties than one may naively expect. The important result in both cases is that superposition of the singular beams can generate additional vortices relative to the vortex content of the initial fields. The relative amplitude and phase difference, and the axes separation, was found to dictate the number and position of new dislocations.

In this paper we investigate the features of the interaction of noncoaxial waves propagating in a weakly nonlinear quadratic crystal. This problem belongs to the broad topic of ''interaction of coupled waves,'' and thus the results found here are expected to be relevant to a variety of other media. For example, the coupling of the waves may be originated due to parametric three-wave interaction, gyrotropy between orthogonal components of an electric field in dielectrics or of a magnetic field in ferrites, or as a result of a Bragg resonance in periodically inhomogeneous media as in, for example, photonic crystals. In all such cases, the waves are coupled and thus follow equations similar to those studied here.

As already mentioned for the three-wave mixing case, in the presence of coupling the waves interchange power and phase, and as a result, each wave consists of the sum of its original vortex and the one transferred from other component. Their superposition generates dislocations with different charges, symmetries, and locations. In this paper we present a detailed analytical and numerical study of such superposition, and discuss the different existing possibilities to control the output light pattern.

The remaining of the paper is organized as follows. In Sec. II we present the equations and geometries we are going to use in our study. We also show explicitly the similarities between the case of three-wave mixing and gyrotropic media or photonic crystals. In Sec. III we provide a solution of the equations and show that it takes the shape of a superposition of noncoaxial beams. In Sec. IV we perform a comprehensive study of such solution from a general point of view. We mainly consider here the superposition of initially equally charged (plus-plus) single vortices separated from each other, but also present some results for the case of oppositely charged (plus-minus) singularities. In the plus-plus case one-three singularities settle at a circle, the radius and the center of which depend on the phases and the amplitudes of both initial vortices. Plus-minus superposition gives hyperbolas

*Electronic address: aps@nls.phys.msu.su
†Electronic address: molina@tsc.upc.es

for two-four vortices disposition. Finally, in Sec. V we use all the acquired knowledge to understand the evolution of two separated vortices and a low-frequency pump in a three-wave interaction. As amplitudes and phases vary depending on the distance of propagation, all stages of superposition peculiar to a linear interference of shifted dislocations are consistently studied. Therefore we investigate dependencies of the number and location of generated vortices on the propagation distance. The spatial dynamics of dislocation production and disappearance at difference frequency is presented. The analytical theory and numerical simulation are developed to study coupled vortex interplay. Both approaches give identical results in the case of weak diffraction.

II. VORTEX INTERACTION IN COUPLED WAVES

A. Parametric three-wave mixing

We consider propagation of optical beams with the carrier frequencies ω_j in lossless quadratically nonlinear media. In this case only the frequencies ω_1, ω_2, and $\omega_3=\omega_1+\omega_2$ are considered and generation of other harmonics can be neglected. The total electric field is expressed as

$$\mathcal{E}=\frac{1}{2}\sum_{j=1}^{3}\mathbf{e}_j A_j(x,y,z)e^{i(\omega_j t-k_j z)}+\text{c.c.}, \tag{1}$$

where A_j are the complex amplitudes, z is the propagation distance, x and y are the coordinates in the transverse plane, $\mathbf{e}_j$ are the unit polarization vectors, and k_j are the wave numbers. If the nonlinear interaction is weak, then the beam amplitudes vary slowly, and their evolution can be described by the set of coupled nonlinear equations [18],

$$\frac{\partial A_1}{\partial z}+iD_1\Delta_\perp A_1=-i\gamma_1 A_3 A_2^* e^{i\Delta kz}, \tag{2}$$

$$\frac{\partial A_2}{\partial z}+iD_2\Delta_\perp A_2=-i\gamma_2 A_3 A_1^* e^{i\Delta kz}, \tag{3}$$

$$\frac{\partial A_3}{\partial z}+iD_3\Delta_\perp A_3=-i\gamma_3 A_1 A_2 e^{-i\Delta kz}, \tag{4}$$

where $D_j=(2k_j)^{-1}$ is the diffraction coefficient, $\gamma_j=2\pi\mathbf{e}_1\hat{\chi}^{(2)}\mathbf{e}_2\mathbf{e}_3\omega_j/(cn_j)$ is the nonlinear coefficient, $\hat{\chi}^{(2)}$ is the quadratic nonlinear susceptibility tensor, n_j is the linear refractive coefficient, and c is the speed of light, $\Delta k=k_1+k_2-k_3$ is the wave vector mismatch. Equations. (2)–(4) can also describe type II second-harmonic generation (SHG), if $\omega_1=\omega_2=\omega$ is the fundamental frequency (FF), A_1 and A_2 are the amplitudes of the ordinary and extraordinary polarized FF components, respectively, and A_3 is the amplitude of extraordinary second harmonic component.

Let us now consider the evolution of Gaussian beams with nested vortices which are incident on the boundary of the nonlinear crystal,

$$A_j(x,y,0)=E_j V_j(x,y)e^{i\varphi_{j0}} \tag{5}$$

where

$$V_j=[x-x_j+i\,\mathrm{sgn}(m_j)y]^{|m_j|}e^{-[(x-x_j)^2+y^2]/w_j^2}, \tag{6}$$

x_j is the coordinate of zero field singularity, m_j is the vortex charge, w_j is the beam width, and E_j, φ_{j0} are the initial amplitude and phase of the fields, respectively.

In the following we consider parametric interaction between the vortices nested in the sum-frequency ω_3 and difference-frequency ω_2 components in the presence of a highintensity, undepleted pump wave with frequency ω_1. We have performed direct numerical simulations of Eqs. (2)–(4) with the initial conditions Eq. (5) and Eq. (6).

The variables and parameters appearing in the model equations can be normalized as follows: $D_{jn}=L/(2k_j w_0^2)$, $\gamma_{jn}=\gamma_j E_0 L$, $A_{jn}=A_j/E_0$, $x_n=x/w_0$, $y_n=y/w_0$, $z_n=z/L$, $\Delta k_n=\Delta kL$. Here E_0 and w_0 are the characteristic amplitude and beam width, respectively, L is the characteristic scale of the propagation distance. Only dimensionless normalized units are used in the remainder of the paper, and hereafter we omit the ''n'' subscript in order to simplify the notation.

All the examples presented in the paper were calculated for the following parameter values: $\gamma_1=0.4$, $\gamma_2=0.6$, $\gamma_3=1$, $D_1=0.025$, $D_2=0.017$, $D_3=0.01$, $E_1=1$, $E_2=E_3=0.1$, $w_1=100$, $w_2=w_3=1$, $m_1=0$, $m_2=m_3=1$. By numerical simulation, the intensity and phase distributions over the beam cross section were obtained as a function of the propagation coordinate z for different initial phases, amplitudes, and beam separation.

Typical snapshots of the difference-frequency beam that is obtained are shown in Fig. 1. The intensity distributions are given in the left column, where the larger intensity corresponds to the darker regions. Therefore the vortices appear as bright spot nested in the beam. In the right column we show the corresponding interferograms of the beams with a tilted plane wave, where the vortices appear as a characteristic fork. When the fork tines point downwards, we consider the vortex to carry a positive topological charge, thus when the fork points upwards the vortex carries a negative topological charge. One observes in the plot that, because of the parametric generation, either one or three vortices appear in the beam, as the propagation distance increases. We note that all the vortices move along a circle, whose diameter is equal to the separation between the beam centers. We elaborate more on this property below, and present an illustration in Fig. 2. This case corresponds to a representative, but particular outcome of the wave evolution.

To perform a comprehensive analysis of the general vortex evolution under conditions of undepleted pump, one of our main goals here is to elaborate an approximate analytical theory of the evolution of coupled vortices under approximate, but general simplifications of Eqs. (2)–(4). First, we neglect the effect of diffraction for wide beams.

Second, we note that in the limit of ideal plane waves, if at the medium boundary the pump amplitude E_1 is much larger than the amplitudes of the other waves, i.e., $E_1 \gg E_{2,3}$, then this amplitude relation is preserved at arbitrary distances in the nonlinear medium as follows from the Manley-Rowe relations [19]. For finite, unfocused beams the same conclusion holds in integral form (i.e., for the powers

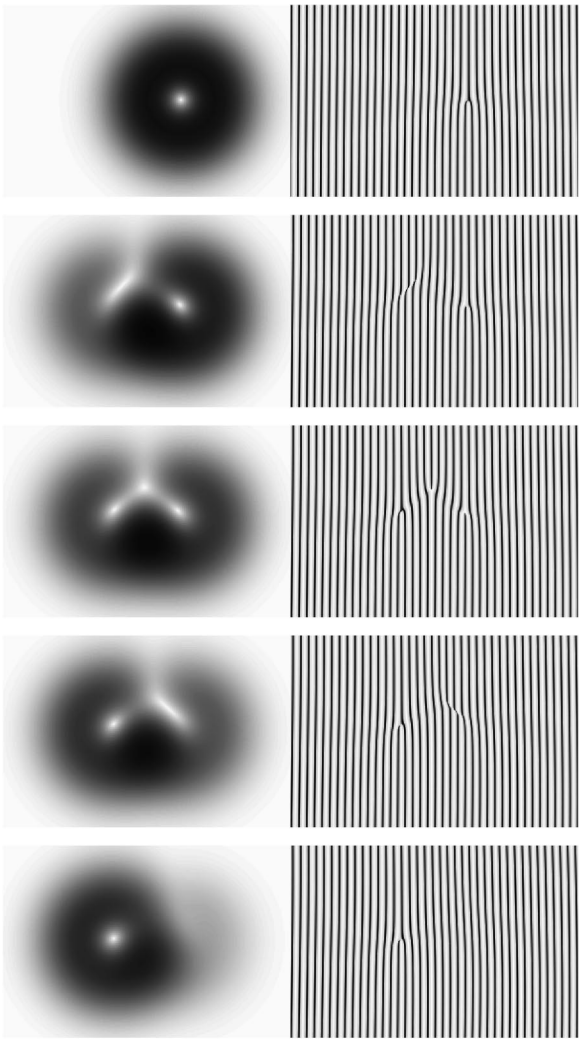

FIG. 1. The intensity distribution (left) and interferogram (right) of the difference-frequency beam are shown at different values of z under parametric interaction between nonaxial beams nested with equally charged $(+1)$ dislocations. The snapshots were obtained by numerical simulation for $x_0=0.7$, and $\varphi_{j0}=0$. They show the main stages of coupled vortices dynamics (from top to bottom as the propagation distance increases):(row 1) the input beam, (row 2) buildup of two new dislocations, (row 3) three symmetric singularities, (row 4) vortex-pair collision, and (row 5) vortex switching to specular position. The detailed evolution of the vortex coordinates is shown in Fig. 7(b).

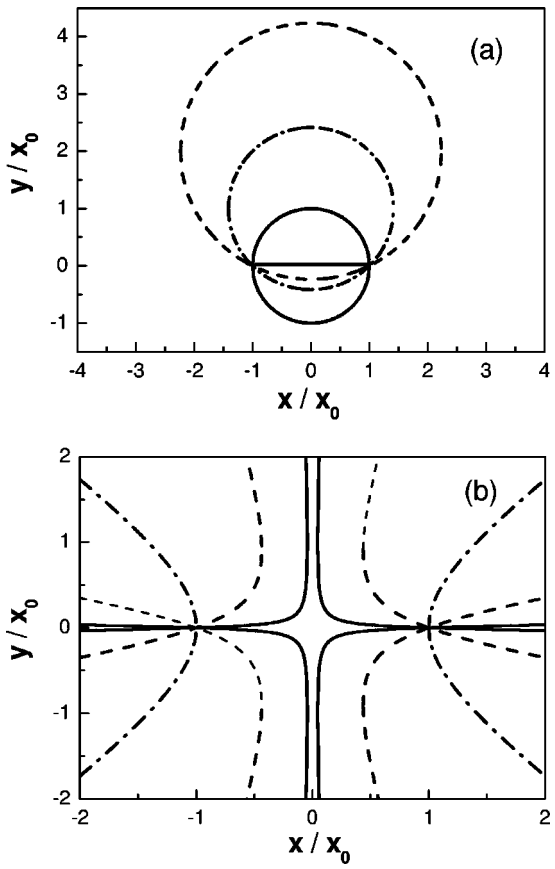

FIG. 2. Location of points in the transverse plane where vortices appear due to superposition of input plus-plus (a) and plus-minus (b) screw dislocations for different values of phase difference φ. The circles (a) correspond to $\varphi=\pi/2$ (solid curve), $\pi/4$ (dash-dotted curve), and 0.45 (dashed curve). The hyperboles (b) are to $\varphi=\pm 0.045$ (solid curve), ± 0.45 (dashed curve), and $\pi/2$ (dash-dotted curve).

carried by each wave). Therefore, in this case the self-action of pump wave is weak and the effect of the nonlinear term in Eq. (2) can be neglected, that is, we can perform analytical analysis using the undepleted pump approximation. Then, interaction of vortices is described by the coupled equations. (3) and (4), where parametrical coupling depends on the amplitude of the pump wave $A_1(x,y,z)$.

In order to reveal the features appearing due to the superposition of vortices in the sum-frequency (ω_3) and difference-frequency (ω_2) waves, we consider the pump beam without dislocations, $m_1=0$. To obtain analytical results, we also assume that the beam width is large so that the variations of the transverse profile in the pump wave can be neglected, so that $V_1\simeq 1$ and $A_1\simeq A_1(x,y,0)\simeq$const. In particular, the analytical theory enables us to construct the domains for one-three and two-four vortices in the parametric plane defined by the amplitude ratio and the phase difference. We will also present later a comparison between our analytical model and the actual numerical results.

B. Vortices in gyrotropic media and spatial uniform coupling

We note that Eqs. (3) and (4) can also describe propagation of wave beams in photonic crystals, and gyrotropic media. In this case the amplitudes A_2 and A_3 correspond to the components of the monochromatic wave $(\omega_2=\omega_3=\omega)$, $\gamma_2 A_1^*=\gamma_3 A_1=\gamma$ is the spatially homogeneous coupling coefficient, $\Delta k=0$, and $D_2=D_3=D$. Therefore, many of the effects predicted for parametrically coupled vortices in field of intense low-frequency pump with the plane-wave transverse profile can also be observed with vortex excitations in magneto-optic and periodically inhomogeneous media.

Recall that the normal waves in gyrotropic media may have left or right circular polarizations [20]. These waves can be represented as a superposition of two linearly polarized

components with the relative phase shift $\pi/2$ or $-\pi/2$, respectively, i.e., we have

$$A^{\pm}=A_2\pm A_3. \tag{7}$$

In order to derive the governing equation for the amplitudes of the normal modes, we substitute Eq. (7) into Eqs. (3) and (4) taking into account restrictions on the parameter values outlined in the beginning of this subsection, and finally obtain the following equations:

$$\frac{\partial A^{\pm}}{\partial z}+iD\Delta_{\perp}A^{\pm}=\mp i\gamma A^{\pm}. \tag{8}$$

Since Eqs. (8) for the two normal mode amplitudes are not coupled, the corresponding solutions can be found independently, and then according to Eq. (7) solution in the original variables is $A_2=(A^{+}+A^{-})/2$ and $A_3=(A^{+}-A^{-})/2$. We see that in a gyrotropic medium vortex transforms from one linearly polarized component to the other one with orthogonal polarization, and vice versa. Therefore, one can observe dynamical transformation of vortices along the propagation direction.

III. ANALYTICAL SOLUTION IN THE WEAK DIFFRACTION LIMIT

We start with the investigation of the beam dynamics for propagation distances smaller than the diffraction lengths of all the interacting waves $l_{dj}=k_j w_j^2/2$, i.e., for $D_j z\ll 1$. Then, the model equations (3) and (4) can be further simplified by removing the diffraction terms, and we finally obtain

$$\frac{\partial A_2}{\partial z}=-i\gamma_2 A_3 A_{10}^{*}e^{i\Delta kz},$$
$$\frac{\partial A_3}{\partial z}=-i\gamma_3 A_2 A_{10}e^{-i\Delta kz}. \tag{9}$$

We find that Eqs. (9) with the boundary conditions (5) have exact analytical solutions for the amplitude of the difference-frequency wave,

$$A_2=\left[A_{20}\cos(\Gamma z)-i\frac{\Delta kA_{20}+2\gamma_2 A_{30}A_{10}^{*}}{2\Gamma}\sin(\Gamma z)\right]e^{i\Delta kz/2}. \tag{10}$$

Here $A_{j0}=A_j(x,y,0)$ is the input amplitude profile [see Eq. (5)], $\Gamma=[\gamma_2\gamma_3E_1^2+(\Delta k/2)^2]^{1/2}=\pi/L_{\mathrm{p}}$, where we introduced the spatial parametric beating length L_p.

The expression for the amplitude profile of the sum-frequency wave can be obtained by exchanging the indices $2\leftrightarrow 3$, and inverting signs in front of Δk, and removing the conjugation mark of pump wave amplitude as $A_{10}^{*}\rightarrow A_{10}$ in Eq. (10).

According to Eq. (6), both A_2 and A_3 contain vortices at the input face of the crystal. Due to the parametric wave mixing taking place inside the nonlinear medium, these vortices penetrate to other components as it follows from Eq. (10). The field in both components is found as a linear superposition of vortices. This kind of field was studied in a previous work [17], and it was found that the topological content of the field may change depending on the relative amplitude and separation distance of the overlapping fields. In the case of parametrical coupling the ratio of the generated and host beam amplitudes, β_c, varies along the propagation distance, and then we expect a rich topological dynamics to occur. In order to determine the positions of new vortex dislocations, we should find zeros of the amplitude profile given by Eq. (10). Then, we conclude that the vortex coordinates satisfy the following transcendental equation

$$V_2(x-x_0,y)+\beta_c(z)V_3(x+x_0,y)=0, \tag{11}$$

where $\beta_c=\beta e^{i\varphi}$ is a complex value of amplitude ratio. Equation (10) gives

$$\beta_c=\frac{-i\gamma_2E_1E_3\exp(i\varphi_0)\sin(\Gamma z)}{\Gamma E_2[\cos(\Gamma z)-i(\Delta k/2\Gamma)\sin(\Gamma z)]}, \tag{12}$$

where $\varphi_0=\varphi_{30}-\varphi_{10}-\varphi_{20}$ is the initial phase difference. We assume, with no lack of generality, that $x_2=-x_3=x_0>0$, since the pump wave does not contain a vortex.

IV. GENERIC SUPERPOSITION OF NONCOAXIAL COHERENT VORTICES

In this section, we discuss the general properties of vortices, which appear due to superposition of two noncoaxial Gaussian beams. We consider two cases, when the beams have their own dislocations with either equal or opposite topological charges. First, the general Eqs. (6) and (11) are used to find analytical expressions for the vortex coordinates. It is clear that the number of solutions of these equations defines the number of generated vortices. Moreover, employing Eq. (6), we establish a simple rule for determining the topological charges of the appearing dislocations. We plot domains in the parameter space amplitude versus phase difference, corresponding to different numbers of dislocations, for various separations between the centers of input beams. Then, we consider examples of vortex dynamics as the amplitudes and phases of superimposed beams changes due to wave mixing.

A. Number of generated vortices, their positions, and topological charges

First of all we consider the case of single charge, equal vortices at the input, $m_2=m_3=1$. Then, we substitute the amplitude profiles given by Eq. (6) into Eq. (11), and derive the following algebraic equation for the coordinates of vortex centers:

$$(x-x_0+iy)e^{2xx_0}+\beta_c(x+x_0+iy)e^{-2xx_0}=0. \tag{13}$$

Separating the real and imaginary parts in Eq. (13), we obtain

$$x\cosh G+x\cos\varphi=x_0\sinh G,\quad G=4xx_0-\ln\beta, \tag{14}$$

$$x^2+(y-x_0\cot\varphi)^2=x_0^2\sin^{-2}\varphi. \tag{15}$$

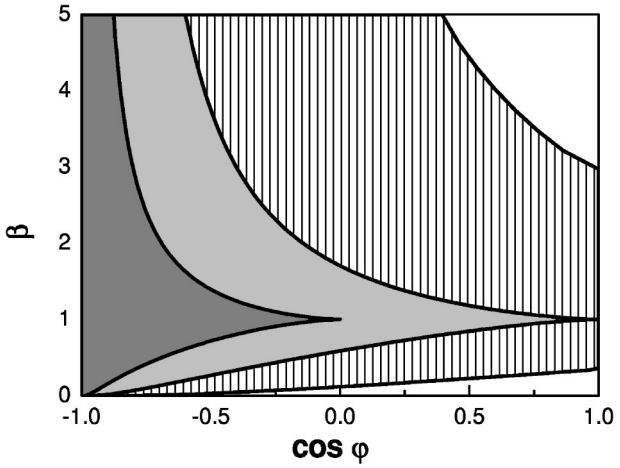

FIG. 3. Domains of three vortices generated by coupled plus-plus screw dislocations for the original displacements $x_0=0.5$ (dark gray), $1/\sqrt{2}$ (gray), 1 (crosshatched).

Note that Eqs. (14) and (15) are simplified to $x=x_0\tanh G$, $x^2+y^2=x_0^2$ for $\cos\varphi=0$, $x=x_0\tanh(G/2)$, $y=0$ for $\cos\varphi=1$, and $x=x_0\coth(G/2)$, $y=0$ for $\cos\varphi=-1$. Equation (15), in particular, proves at once that x coordinates of arising vortices are limited by value $x_0/|\sin\varphi|$. According to Eq. (15), the dislocations appear on a circle with the radius $x_0/|\sin\varphi|$, and with the center in a point $(0,x_0 cot\,\varphi)$, as shown in Fig. 2. The circle always passes through initial points $(x_0,0)$ and $(-x_0,0)$. In the case of $\pi/2$, the circle center is located at the origin, see the solid curve in Fig. 2(a). The corresponding dynamical transformations of vortices are shown in Fig. 1. The circle moves upwards, and the radius becomes larger as φ increases. It degenerates to straight lines $y=0$ and $y\to\infty$ when $\cos\varphi=-1$.

Thus the generated vortices are placed on the circle at the beam cross section. There are one or three vortices depending on the beam distance x_0, the amplitude ratio β, and the phase difference φ. We can find the boundary of the three-vortex domain in the following way. Such domain is placed between the vertical tangents to the curve $x=x(\beta)$. To determine their positions, it needs differentiating Eq. (14) with respect to x. The obtained expression must be solved jointly with Eqs. (14). Having fulfilled such procedure and carried out simple algebraic transformation, we find the following equations for curves that define the three-vortex domains:

$$\beta_b=\exp(4x_bx_0)\left(\frac{4x_b^2-4x_bx_0+1}{4x_b^2+4x_bx_0+1}\right)^{1/2}, \tag{16}$$

$$\cos\varphi_b=\frac{4x_0^2-4x_b^2-1}{[(1+4x_b^2)^2-16x_b^2x_0^2]^{1/2}}. \tag{17}$$

The three-vortex domains constructed by Eqs. (16) and (17) are shown in Fig. 3 for different beam separation x_0. The domain has the extreme point of a cusp type at

$$\cos\varphi_{ex}=4x_0^2-1 \tag{18}$$

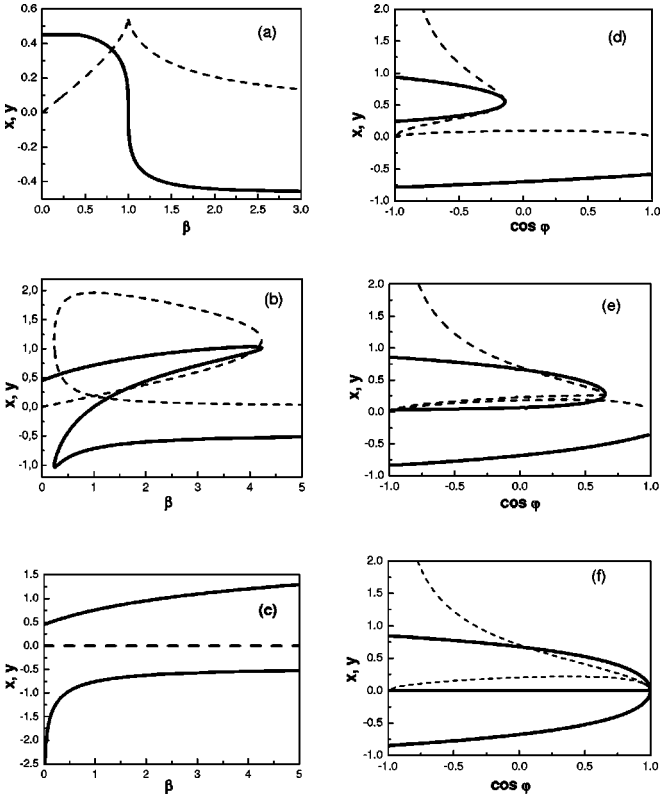

FIG. 4. Vortex coordinates x (solid curves), y (dashed curves) as a function of the amplitude ratio β for $x_0=0.45$ (left column) and of the phase difference φ for $x_0=1/\sqrt{2}$ (right column) in case of plus-plus interaction. The parameter $\cos\varphi=-0.19$ (a), -0.9 (b), -1 (c), and $\beta=2$ (d), 1.1 (e), 1 (f). The plots are obtained by analytical solution of Eqs. (16) and (17).

and lays in the straight line $\beta=1$. Only one positive vortex exists outside the domain. In the domain topological charges of three vortices alternate as plus, minus, and plus. Interestingly, the vortex characteristics with β are the same as with $1/\beta$ when a phase difference is fixed.

B. Dependence of vortex positions on the amplitude-phase relations

Let us now consider representative examples of vortex superposition while the amplitude ratio changes, see Fig. 4 (left column). The two limiting cases, when β approaches zero and when β goes to infinity, correspond to the cases when only one of the two overlapping fields is present in the total field. One expects in those cases only one vortex to be present in the field, and its location should be that of the corresponding beam, either $(x_0,0)$ or $(-x_0,0)$. As an example we have chosen beams separated on the distance $x_0=0.45$ at which the extreme point of the domain is $\cos\varphi_{ex}=-0.19$.

We start our analysis with the critical case $\varphi=\varphi_{ex}$. Here, as mentioned above, only a single vortex exist for the whole range of amplitudes, but its position changes while changing the relative amplitudes. It is in this range that the singularities switched from initial position $(x_0,0)$ to opposite point $(-x_0,0)$ under the monotonic amplitude ratio increase, as

shown in Fig. 4(a). The vortex moves on a circular arc, and the maximum remoteness along y axis is $y_m = x_0 \tan(\varphi/2) = 1.21 x_0 = 0.545$ at $x = 0$.

When the relative phase is such that its cosine is less than the extreme value $\cos\varphi < \cos\varphi_{ex}$, three vortices can arise. We consider more particularly the case of $\cos\varphi = -0.9$, see Fig. 4(b). The three-vortex region begins at $\beta_{b2} = 1/\beta_b = 0.23$ and ends at $\beta_{b1} = \beta_b = 4.25$.

The initial vortex is displaced away from the origin along both axes while increasing the relative amplitude. It reaches the farthest position $x_{m1} = 1.03$ at $\beta_m = 4.25$. A vortex twin is created at the point $x_{m2} = -x_{m1}$ when $\beta = \beta_{b2}$. The positive vortex of the twin moves towards the position $(-x_0, 0)$ which corresponds with the center of one of the original fields, V_3. Its negative counterpart moves to collide with the initial vortex. They annihilate each other at $\beta = \beta_{b1}$, leaving only a single vortex in the field. One can see that the whole process is symmetric when one changes β to $1/\beta$.

The case $\cos\varphi = -1$ is degenerate. Here, only two positive vortices appear for the whole range of β, but at the boundary points $\beta = 0$ and $\beta \to \infty$ where, as only one field contributes to the sum, only one vortex is present. The new positive vortex enters in the total field from afar. The negative vortex goes to infinity along y axis. A representative example is shown in Fig. 4(c).

We have also studied how the vortex positions change with relative phase variations, when the amplitude is fixed. In Figs. 4(d–f) we present some representative cases, where the separation distance is fixed to $x_0 = 1/\sqrt{2}$, which is the critical distance, thus regions with three vortices will appear at any amplitude ratio. As can be seen from Fig. 3, when $\beta = 1$ the three vortices region covers the whole phase domain, as shown in Fig. 4(f). The larger the departure of the amplitude from unity, the smaller is the three vortices region.

Investigation of beam separation influence on plus-plus vortex superposition was performed theoretically and experimentally in Ref. [17]. Thus we omit such discussion.

C. Superposition of vortices with opposite topological charges

Similar features appear for superpositions of vortices with different charges, although the actual dynamics and number of vortices change from case to case. Because of this, we have also studied the superposition where the vortices of the overlapping fields have opposite charges: $m_2 = 1, m_3 = -1$. In this case only two or four vortices can appear. In Fig. 5 we present the domains in the parameter space where four vortices appear. Only two vortices can be found outside the domains. Analytical expressions for this case can also be found and, for example, the parametric equations for the boundary between the domains are

$$\beta_b = \exp(4x_b x_0)\left(\frac{4x_0^2 - 4x_b x_0 - 1}{4x_0^2 + 4x_b x_0 - 1}\right)^{1/2}, \tag{19}$$

$$\cos\varphi_b = \frac{4x_0^2 - 4x_b^2 - 1}{[(1+4x_0^2)^2 - 16x_b^2 x_0^2)]^{1/2}}. \tag{20}$$

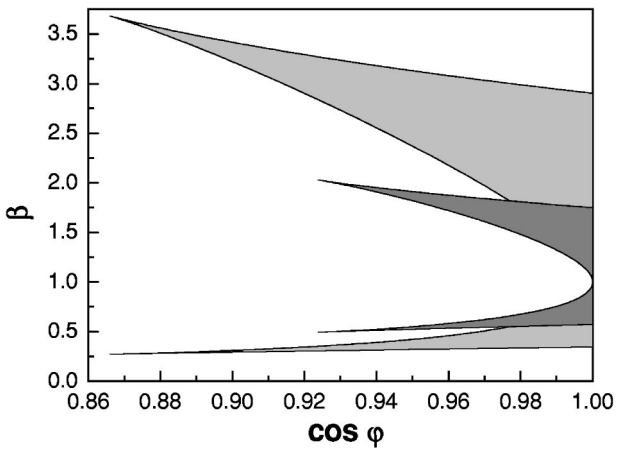

FIG. 5. Domains of four vortices generated by plus-minus screw dislocations for the original displacements $x_0 = 0.9$ (dark gray filling), 1.0 (gray filling).

The extreme points of the domain are located in

$$\cos\varphi_{ex} = (4x_0^2 - 1)^{1/2}/(2x_0^2), \tag{21}$$

and if the beam separation is less than the critical value $x_{cr} = 1/\sqrt{2}$, the four-vortex domains disappear. Within such domains the topological charge alternates as plus, minus, plus, minus from one vortex to another.

The equations which govern the position of the vortices are

$$x_0 \cosh G + x_0 \cos\varphi = x \sinh G, \quad G = 4x x_0 - \ln\beta, \tag{22}$$

$$y^2 + 2xy \cot\varphi - x^2 + x_0^2 = 0 \tag{23}$$

and some representative cases are shown in Fig. 6.

We emphasize that one of two positive vortices goes to y infinity when $\cos\varphi = 1$, see Figs. 6(c,e). In that case Eqs. (22) and (23) become $x = x_0 \tanh(G/2)$, $y = 0$ for remaining vortices.

V. SPATIAL DYNAMICAL EVOLUTION OF COUPLED VORTICES

In this section we focus on the case of equal vortices and their propagation in nonlinear quadratic media. We analyze the dynamics of the vortices in the difference-frequency component A_2, when the initial fields A_2 and A_3 contain vortices of the same sign $m_2 = m_3 = 1$. We will use the analytical results obtained in Sec. III in two distinct cases: (i) exact phase matching $\Delta k = 0$ and (ii) large phase mismatch $|\Delta k| \gg \Gamma_0$. The first case also corresponds to vortex excitations in gyrotropic medium (see Sec. II B).

In our analytical development, we have neglected the effect of beam diffraction. In order to determine the evolution under weak diffraction, and its influence on our results, we have performed direct numerical simulations of Eqs. (2) and (4) with the boundary conditions Eq. (5) and Eq. (6). A comparison between analytical and numerical simulation results is given below.

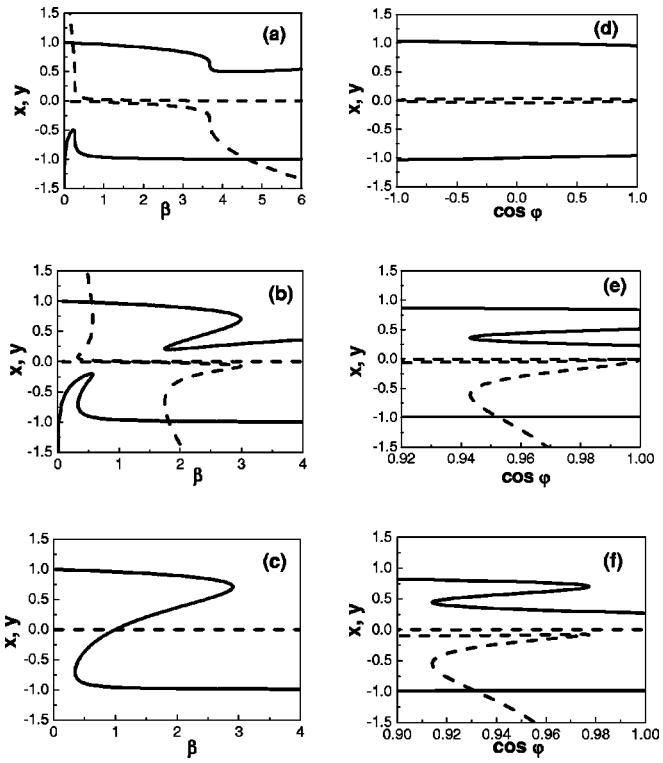

FIG. 6. Vortex coordinates x (solid curves), y (dashed curves) vs the amplitude ratio β (left column), and the phase difference (right column) for supercritical initial separation $x_0=1$ of plus-minus screw dislocations. The parameter $\cos\varphi=0.866$ (a), 0.98 (b), 1 (c), and $\beta=1$ (d), 2.5 (e), 3 (f). The plots are obtained by analytical solution of Eq. (22).

A. Vortex mixing at phase matching

According to the analytical solution (12) obtained in the nondiffraction limit [model Eqs. (9)], the phase difference between the second and third components does not change in the case of phase matching $\Delta k=0$, and remains the same as at the input. Then, using Eq. (12) we can obtain simplified expressions of the amplitude ratio and phase difference for the generated and host beams,

$$\beta=\beta_m|\tan(\Gamma_0 z)|,\quad \cos\varphi=\mathrm{sgn}[\tan(\Gamma_0 z)]\sin\varphi_0, \quad (24)$$

where $\beta_m=(\gamma_2/\gamma_3)^{1/2}E_3/E_2$. As will be shown explicitly for the case of phase mismatched waves, these kind of equations define a curve in the phase space $[\beta,\cos(\phi)]$. The crossings of this curve with the boundaries of the domains in Fig. 3 are the points where creation or annihilation of vortices occur. From Eq. (24) it is seen that the host amplitude vanishes at half the beating length $L_p=\pi/(2\Gamma_0)$. Note that β goes through all possible values while changing the propagation distance inside the crystal. According to Eq. (24) the phase difference jumps by π occur because of changing sign of $\tan(\Gamma_0 z)$.

We first study parametric mixing of dislocations when $\varphi_0=0$, so that $\cos\varphi(0)=0$, see Eq. (24). In this case the vortices are situated at the circle $x^2+y^2=x_0^2$, Eq. (14). If original vortices are less than a critical distance apart, which is $x_{cr}=1/\sqrt{2}$ for this particular case, only a single dislocation

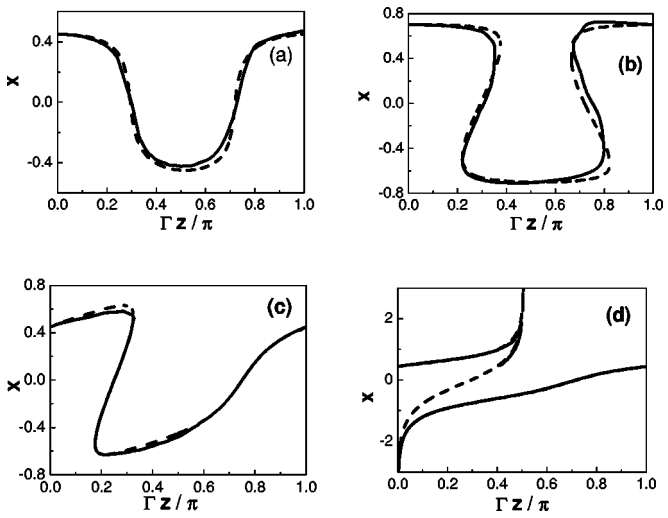

FIG. 7. Dependence of difference-frequency vortex coordinate x on the propagation distance z under phase matching. The parametric superposition occurs between two beams with $\beta_m=1$, and (a) $x_0=0.45$, $\varphi_0=0$; (b) $x_0=0.7$, $\varphi_0=0$; (c) $x_0=0.45$, $\varphi_0=-\pi/3$; and (d) $x_0=0.45$, $\varphi_0=-\pi/2$. Solid line is the result of numerical simulation, dashed line is the analytical solution of Eqs. (14) and (24).

is formed, see Fig. 7(a) where we have used $x_0=0.45$. In this case, the vortex goes from $(x_0,0)$ to $(-x_0,0)$ passing through the point (0,0), where $\beta=1$, at the length $z_0=\Gamma_0^{-1}\tan^{-1}(1/\beta_m)=0.25L_p$ and reaches opposite side $x_0=-0.45$ at the distance $z_p=0.5L_p$, where the energies of the A_2 and A_3 beams are exchanged. After this cycle the similar process is repeated in contrary transverse direction. The numerical simulations are in good agreement with the result of our analytical model.

When the beam separation is larger than the critical distance three vortices can be generated. In Fig. 7(b) we show a typical example for $\varphi_0=0$ and $x_0=0.7>0.5$. We observe that, besides the original vortex, a new twin of vortices is created at about $z_{b1}\simeq 0.2L_p$. One of them collides with the original vortex, annihilating each other at $z_{b2}=\Gamma_0^{-1}\cot^{-1}(\beta_m/\beta_b)\simeq 0.38L_p$. The remaining positive charged vortex moves towards the position $(-x_0,0)$. It reaches that position when the exchange of energy is complete. After that point the process in Fig. 7 repeats itself. Characteristic examples of direct numerical simulations are presented in Fig. 1. These plots demonstrate that the amplitude and phase profiles can be used to determine the vortex positions, and determine the topological charges of dislocations. Results of such numerical calculations are plotted with solid curves in Fig. 7.

The dynamics of the vortices is modified if we use other initial phase mismatches. For instance, introducing $\varphi_0=-\pi/3$, and hence $\cos\varphi(0)=-0.5$ the symmetric trajectory of parametric vortex is distorted as it is shown in Fig. 7(c). the asymmetry results from the phase difference jump by π at $z=\pi/(2\Gamma)=0.5L_p$ according to Eq. (24). Here we have kept all the other parameters used for the simulation identical to those in Fig. 7(a).

B. Effects of weak diffraction

There is a large change in the pattern when we set $\cos\varphi(0)=-1$, see Fig. 7(d). If we tune the initial phase to be $\varphi_0=-\pi/2$ we expect to achieve the desired conditions. Indeed, initially we see only two trajectories, which correspond to two branches in Fig. 4(e). However, at a larger distance, $z\simeq 0.4L_p$, the third vortex appears in between the first two. This happens due to the *diffraction-induced phase mismatch*. Let us study these effects in more detail. The parameters of a wave beam are modified as a result of diffraction. In the linear diffraction regime, the beam width increase is proportional to the factor $f=(1+z^2/L_{dj}^2)^{1/2}$, the phase front becomes curved, where the curvature radius is $R=z+L_{dj}^2/z$, and the phase shift is accumulated at the beam axis, $\varphi_d=\cot^{-1}(z/L_{dj})$. At small propagation distances, $z\ll L_{dj}$, the additional phase, which is accumulated due to diffraction, is proportional to the distance, i.e., $\varphi_d\simeq z/L_{dj}$. Such a linear increase of phase corresponds to an effective increase of the beam phase velocity, and the decrease of the wave number by

$$\Delta k_{dj}\simeq -1/L_{dj}=-4D_j/w_j^2. \tag{25}$$

The three-wave interaction is primarily influenced by the presence of the diffraction-induced wave number mismatch, $\Delta k_d=\Delta k_{d1}+\Delta k_{d2}-\Delta k_{d3}$, which can be presented, using Eq. (25), in the following form:

$$\Delta k_d=4(D_3/w_3^2-D_2/w_2^2-D_1/w_1^2). \tag{26}$$

Small variations of beam width and the curvature of the phase front can be neglected, provided that the condition $z\ll L_{dj}$ is satisfied. Then, the leading order correction to the wave number mismatch is given by Eq. (26).

For the case of Fig. 7(d), the diffraction-induced mismatch is $\Delta k_d\simeq -0.11/L_p$. As we have already mentioned, the case with $\cos\varphi=-1$ is a degenerate one, and even such a small perturbation will change the expected two-vortex regime. Instead, we have the usual one- and three-vortex domains. The vortex with negative sign appears in the simulation window at $z\simeq 0.4L_p$, and annihilates with the original vortex at $z\simeq 0.5L_p$.

Note that, if initial dislocations are not in phase, they move in a spiral, which is projected in a circle at beam cross section according to Eq. (15).

C. Vortex mixing under phase mismatch

Under the presence of a phase mismatch between the parametrically coupled waves $(\Delta k\neq 0)$, the phase difference between the superimposed vortices φ varies along the propagation distance as follows from Eq. (12). Then, the spatial dynamics of vortices becomes more complicated compared to the case of exact phase matching considered earlier in Sec. V A. If the phase mismatch is large, $|\Delta k|\gg\Gamma_0$, then Eq. (12) can be simplified and we obtain the relations

$$\beta(z)=\beta_{mm}|\sin(\Delta kz/2)|, \tag{27}$$

$$\cos\varphi(z)=\mathrm{sgn}[\sin(\Delta kz/2)]\sin(\varphi_0+\Delta kz/2),$$

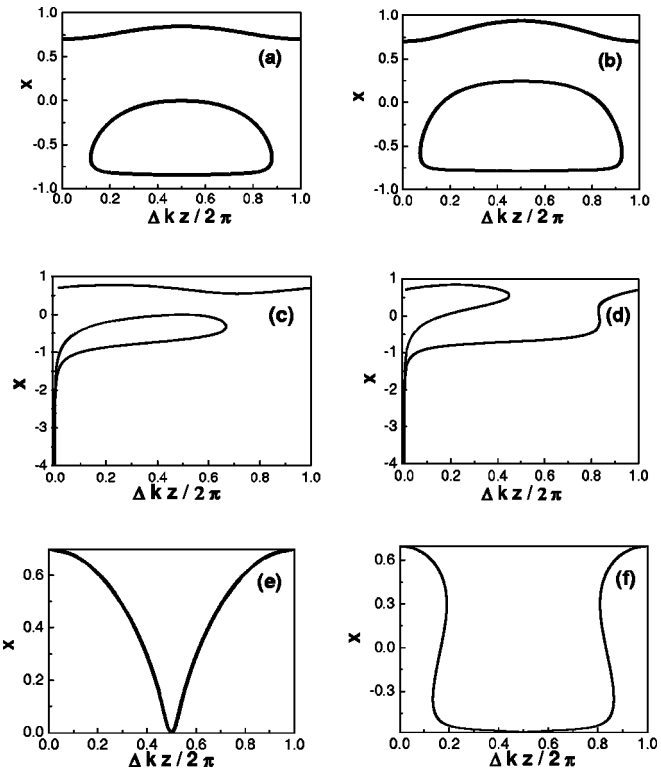

FIG. 8. Dependence of difference-frequency vortex coordinate x on the normalized propagation distance $\Delta kz/2\pi$ when $x_0=0.7$. Upper row, $\varphi_0=\pi$; middle row, $\varphi_0=-\pi/2$, and bottom row, $\varphi_0=0$. Left column, $\beta_{mm}=1$ and right column, $\beta_{mm}=2$. Other parameters are given in the beginning of Sec. V.

where $\beta_{mm}=(2\gamma_2E_1/|\Delta k|)(E_3/E_2)$ is the maximum achievable amplitude ratio along the propagation distance z. It follows from Eq. (27) that the relative amplitude between the superimposed vortices oscillates along the propagation distance with the spatial period $L_p=2\pi/|\Delta k|$, and phase difference experiences the jump by π in each spatial period. Strong penetration of the guest beam is observed if β_{mm} is large, and this regime can be realized by increasing the amplitude of the third wave E_3. We note, however, that these results are obtained in the frames of the undepleted pump approximation, which is valid if the condition $E_3\ll E_1$ is satisfied.

In order to determine the positions of the generated vortices, we substitute Eq. (27) into the general expression Eq. (14), and obtain the following relation between the vortex coordinates x and the propagation distance z,

$$\tan(\Delta kz/2)=\frac{(x-x_0)\exp(4xx_0)}{-\beta_{mm}x\sin\varphi_0\pm[\beta_{mm}^2x_0^2-F^2]^{1/2}}, \tag{28}$$

$$F=(x_0-x)\exp 4xx_0+\beta_{mm}x\cos\varphi_0.$$

In Fig. 8 we present the analytical calculations of the vortex coordinates while the propagation distance increases. If $\varphi_0=\pi$ (upper row) a single vortex appears in the first steps of propagation. This host vortex moves away from the central region to the beam periphery. At larger propagation

distance the phase difference φ continues to increase, and three singularities appear. Then, the process goes in the reverse direction. If the coefficient β_{mm} is increased, the three-dislocation domain becomes larger along the z axis, compare Fig. 8(b) with Fig. 8(a).

We now consider an interesting case, $\varphi_0=-\pi/2$ when $\varphi(0)=\pi$ and the appropriate examples are presented in the middle row of Fig. 8. Near an input three vortices are excited: one in the central region, and two more at the beam periphery. Under amplitude balance condition $\beta_{mm}=1$, these two vortices move towards the central region, then merge and disappear, see Fig. 8(c). However, if β_{mm} is large, the middle vortex moves towards the host one, and they fuse and disappear, as shown in Fig. 8(d).

The out-of-phase beams ($\varphi_0=0$) can excite one or three dislocations, see bottom row in Fig. 8. At amplitude balance $\beta_{mm}=1$ one vortex appears, see Fig. 8(e). It is attracted towards the beam which penetrates from the sum-frequency component. However, if β_{mm} is large, then three vortices can be excited, Fig. 8(f). In two last cases vortex reaches extreme position at the distance $z=L_p/2$, and then returns to the original position.

D. Vortex trajectories on the amplitude versus phase parameter plane

The coordinates of generated vortices change in the process of wave mixing, due to the changes of amplitudes and phases during the beam propagation, as we have illustrated in Sec. V C. If one want to determine just the number of generated vortices, then this can be predicted more easily, by analyzing the result of wave mixing in the parameter plane (β,cos ϕ). We have demonstrated earlier that these parameters uniquely determine the number of vortices, for a fixed distance between the input beams, as illustrated in Fig. 8. However, Eqs. (27) give the following relation between these parameters for three-wave interaction under phase mismatching

$$\cos\varphi=\frac{\beta\cos\varphi_0}{\beta_{mm}}+\mathrm{sgn}[\sin(\Delta kz)]\sin\varphi_0\left[1-\frac{\beta^2}{\beta_{mm}^2}\right]^{1/2}, \tag{29}$$

which describes a line in Fig. 3. If such a line crosses the shaded domain, three dislocations are generated at some distances.

Let us illustrate the results for the beam separation parameter $x_0=0.7$. In Fig. 9, we plot the corresponding three-soliton domain from Fig. 3, and also draw characteristic trajectories defined by Eq. (29). These curves correspond to the different values of mismatches, which we choose to be the same as in Figs. 8(a–f). Full coincidence between the full and simplified descriptions is evident. For example, the trajectory (e) for $\varphi_0=0$ does not cross the three-vortex domain in Fig. 9, and we see only one vortex generation in Fig. 8(e). If an energy exchange is increased up to $\beta_{mm}=2$, the corresponding trajectory (f) crosses this domain, and there are regions of three-vortex generation in Fig. 8(f). If the initial phase difference becomes equal to $-\pi/2$, then the trajectories in Fig. 9 always cross the three-vortex domain. The larger the amplitude ratio β_{mm}, the longer is the distance where three vortices exist, cf. the cases (c) and (d). To summarize, the trajectories plotted on a parametric plane in Fig. 3 enable us to quickly reveal the qualitative dynamics of three-wave vortex generation.

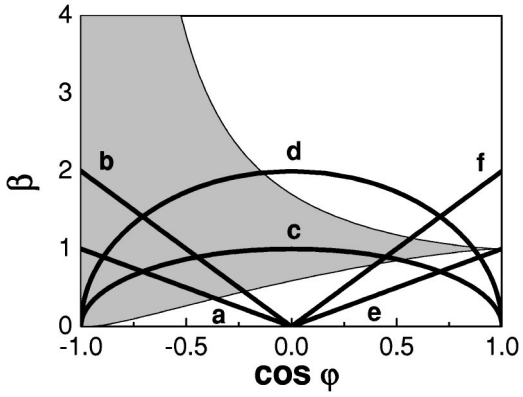

FIG. 9. Vortex trajectories in the parameter plane (β,cos φ) under phase-mismatched interaction of equally charged vortices nested in noncoaxial beams with the separation $x_0=0.7$. The motion along the lines (a–f) corresponds to the changes of vortex coordinates shown in Figs. 8(a)–8(f). Three vortices appear when the parametric trajectory enters the gray shaded region, which was earlier shown in Fig. 3.

The trajectories defined by Eq. (29) can be superimposed in a similar way over the four-vortex domains, shown in Fig. 5 for the case of oppositely charged input beams. In this case the number of vortices will change from two to four (or the other way around), as the domain border is crossed.

VI. CONCLUSIONS

We have reported a detailed study of the mixing of noncoaxial vortices in parametric wave coupling. Our results are applicable to the cases of (i) three-wave parametric interactions in quadratic media, (ii) coupling of orthogonally polarized components in the gyrotropic media, and (iii) wave propagation in photonic crystals under Bragg-resonance conditions. In all such cases, each wave carries its own vortex and the one that is transferred from the other components. The noncoaxial superposition of the singularities gives rise to the appearance of new dislocations with different charges, symmetries, and spatial positions.

We have performed extensive numerical simulations taking into account all the key factors, which govern the interaction of wave beams. Several example illustrate amplitude and phase distributions in the beam cross sections, which were used to determine coordinates and charges of the generated vortices, under different conditions. However, for uniform coupling and negligible diffraction, we have developed an analytical description. The corresponding solution was applied to analyze vortex generation by the separated beams, containing screw phase dislocations with plus-plus and plus-minus topological charges. The equations for the generated vortex coordinates have been obtained.

It has been shown how the number and coordinates of the

generated vortices depend on the beam separation distance, amplitude ratio, and phase difference. For each phase difference a critical value of the beam separation exists. In the case of plus-plus vortices the beams separated large distances can create three vortices simultaneously. Under the amplitude balance one dislocation is always located exactly between two beams. The superposition of unequal vortices gives two or four dislocations. We have found the parameter domains for both one-three and two-four vortices generation. The vortex trajectories were found under phase matching, and large phase mismatch. Here the ranges of one and three vortices periodically replace each other. In addition, numerical simulation of parametric interaction between sum and difference beams with the low-frequency pump wave in a quadratic medium was carried out.

Under weak diffraction and wide pump beam, the simulation data are in a good agreement with the analytical solution, obtained for uniform coupling. Only in a special degenerate case, the dynamics of generated vortices is quite sensitive to even minor changes in the phases of interaction waves. We have demonstrated that this phase mismatch appears due to the diffraction effects, and estimated the induced wave number mismatch.

We conclude by noticing the interest of the extension of the results presented here to the simultaneous frequency conversion and shaping of beams using optical vortices [21–23], to the case of multiple noncoaxial beams, such as those appearing in vortex streets [24], whose signature was observed recently in second-harmonic generation in the presence of significant Poynting-vector walk-off [25], and to the superposition of light beams with more general shapes, light Bessel beams [26].

ACKNOWLEDGMENTS

Authors A.P.S. and A.A.K. acknowledge support from the Russian Foundation for Basic Research under Projects 02-02-17127, 02-02-06531, 02-02-81029, and from the Federal Program ''Support for Leading Scientific Schools'' under Project 00-15-96561. Authors G.M.T. and L.T. were supported by the Generalitat de Catalunya and by the Spanish Government through Grant No. TIC2000-1010.

[1] J.F. Nye and M.V. Berry, Proc. R. Soc. London, Ser. A **336**, 165 (1974).
[2] M.S. Soskin and M.V. Vasnetsov, in *Progress in Optics XLII*, edited by E. Wolf (Elsevier, Amsterdam, 2001).
[3] Yu.S. Kivshar and E.N. Ostrovskaya, Opt. Photonics News **12**, 24 (2001).
[4] I. Freund, Opt. Commun. **159**, 99 (1999).
[5] I. Freund, Opt. Commun. **181**, 19 (2000).
[6] I. Freund, Opt. Lett. **26**, 545 (2001).
[7] V.Yu. Bazhenov, M.V. Vasnetsov, and M.S. Soskin, Pisma Zh. Eksp. Teor. Fiz. **52**, 431 (1990) [JETP Lett. **52**, 429 (1990)].
[8] N.R. Heckenberg *et al.*, Opt. Lett. **17**, 221 (1992).
[9] M.W. Beijersbergen *et al.*, Opt. Commun. **96**, 123 (1993).
[10] I.V. Basistiy *et al.*, Opt. Commun. **103**, 422 (1993).
[11] K. Dholakia *et al.*, Phys. Rev. A **54**, 3742 (1996).
[12] J. Courtial *et al.*, Phys. Rev. A **56**, 4193 (1997).
[13] D.V. Petrov and L. Torner, Phys. Rev. E **58**, 7903 (1998).
[14] A. Stabinis, S. Orlov, and V. Jarutis, Opt. Commun. **197**, 419 (2001).
[15] A. Berzanskis *et al.*, Opt. Commun. **140**, 273 (1997).
[16] M.S. Soskin *et al.*, Phys. Rev. A **56**, 4064 (1997).
[17] G. Molina-Terriza, J. Recolons, and L. Torner, Opt. Lett. **25**, 1135 (2000).
[18] Yu.N. Karamzin and A.P. Sukhorukov, Zh. Éksp. Teor. Fiz. **68**, 834 (1975) [Sov. Phys. JETP **41**, 414 (1975)].
[19] Y.R. Shen, *The Principles of Nonlinear Optics* (Wiley, New York, 1984).
[20] J. Petykiewicz, *Wave Optics* (Kluwer Academic Publishers, Dordrecht, 1992).
[21] G. Molina-Terriza *et al.*, Opt. Express **9**, 110 (2001).
[22] E. Abramochkin and V. Volostnikov, Opt. Commun. **125**, 302 (1996); **141**, 59 (1997).
[23] E.G. Churin, Opt. Lett. **24**, 620 (1999).
[24] J.T. Malos *et al.*, Opt. Lett. **22**, 1056 (1997).
[25] G. Molina-Terriza *et al.*, Opt. Lett. **27**, 625 (2002).
[26] V. Pyragaite *et al.*, Opt. Commun. **198**, 459 (2001).